LBL-12743
Revised

# Lawrence Berkeley Laboratory
UNIVERSITY OF CALIFORNIA

## Physics, Computer Science & Mathematics Division



Presented at the IEEE Nuclear Science Symposium, San Francisco, CA, October 21-23, 1981; and to be published in IEEE Transactions on Nuclear Science, Vol. NS-29, No. 1, February 1982

# CONTRIBUTION OF TIME-OF-FLIGHT INFORMATION TO LIMITED ANGLE POSITRON TOMOGRAPHY

B. Macdonald, V. Perez-Mendez, and K.C. Tam

October 1981



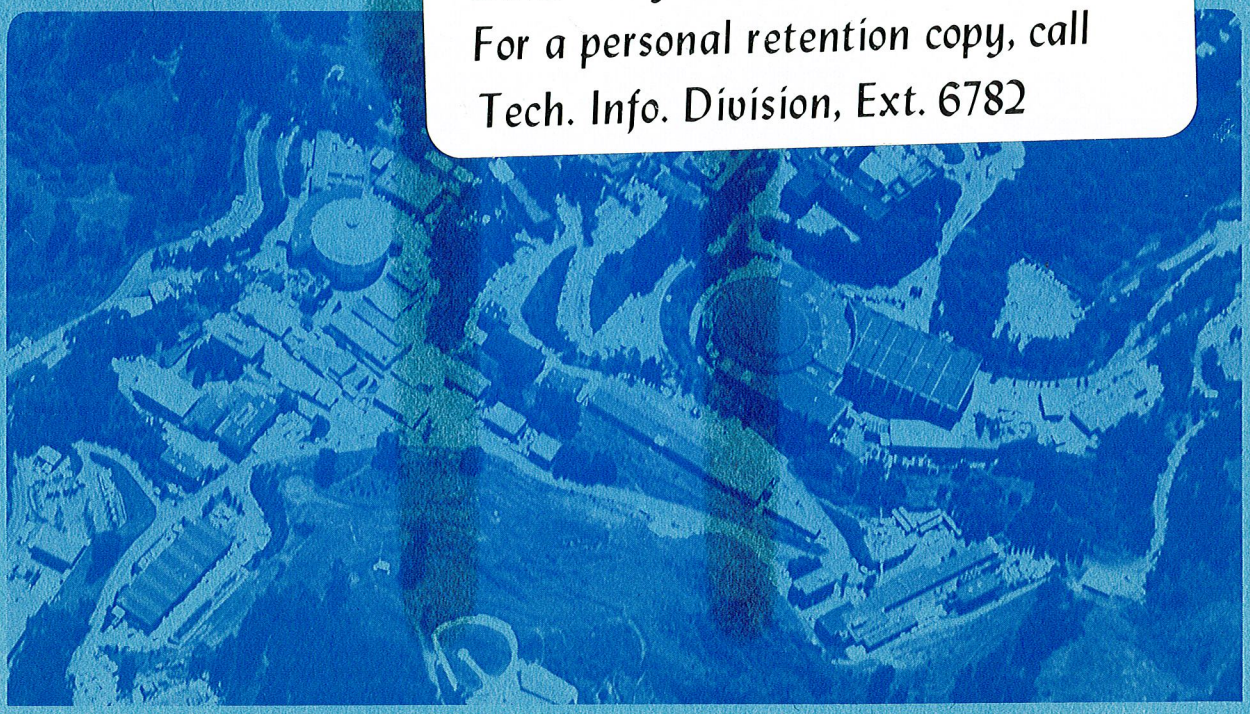

Prepared for the U.S. Department of Energy under Contract W-7405-ENG-48

# CONTRIBUTION OF TIME-OF-FLIGHT INFORMATION TO LIMITED ANGLE POSITRON TOMOGRAPHY

Submitted to IEEE Nucl. Sci. Symp. NS-29, Feb., 1982

B. Macdonald and V. Perez-Mendez
Lawrence Berkeley Laboratory, University of California, Berkeley, CA 94720
and
K.C. Tam
General Electric Research Laboratory, Schenectedy, NY 12345

## Summary

Limited-angle emission tomography has been investigated using a two-dimensional phantom to generate positron events simulating a camera with two opposed parallel position-sensitive detectors collecting data within a 90° cone. The data, backprojected onto lines passing through the phantom volume, is used with a matrix reconstruction method to provide two-dimensional images. Image quality has been measured using the standard deviation of the reconstructions with respect to the original phantom. The application of Phillips-Twomey smoothing to the deconvolution matrices has substantially improved the original reconstructions, a factor of 1.9 in signal to noise ratio, giving S/N = 3.4 for a phantom having an average of 150 events/pixel. Using photon time-of-flight to restrict the reconstruction volume a further considerable improvement is made. When the time-of-flight limited the contributing volume to 4 lines out of 11 the improvement was another factor of 1.9 giving SN = 6.0 for the same phantom. Comparable increases in signal to noise ratios are expected for three-dimensional reconstructions.

## Introduction

Positron emission tomography with currently operating ring cameras has given excellent results because of the cameras' full 360° coverage of the emitting region. It is clear that reconstructions of comparable quality are not possible with limited angle cameras since significant areas of the object's spatial frequencies are measured either not at all or with a large noise magnification. On the other hand, there are certainly a number of applications for which limited angle reconstruction from projections would be useful, for reasons of cost, convenience, or necessity, and for which improvements in image quality would be helpful

We will demonstrate below the increase in image quality possible when limited angle reconstructions are made which maximize smoothness. A further source of image improvement comes from using positron gamma-ray time-of-flight information. Current timing accuracies of about 0.5 nsec localize the positron only to about 7 cm, a figure much larger than current spatial resolutions of about 1 cm. Gamma-ray timing can, however, be used to reduce the source volume contributing to a given reconstruction, increasing the signal/noise ratio. This has been done already for ring camera applications[1] and we shall show the improvement which might be obtained with a limited angle camera.

## Theory

In this paper we have constructed a computer model, in two dimensions, of a large-area positron camera (Fig. 1) which can measure the coordinates $x_a, x_b$ of photons from positron annihilation. Reconstruction of the positron source distribution $\rho_i(x')$ uses back-projection tomograms,[2] the distribution of intersections of event lines $(x_a, x_b)$ with lateral lines through the a priori known area of the source. Since data is collected only in a cone of angle $\Theta$ ($\Theta$ = 45° here) the point response function $h_{ij}(x-x')$ [source point $(x',i)$; tomogram point $(x,j)$] is non-zero only in that cone. The back-projection tomograms $t_j(x)$ are related to the source distribution by

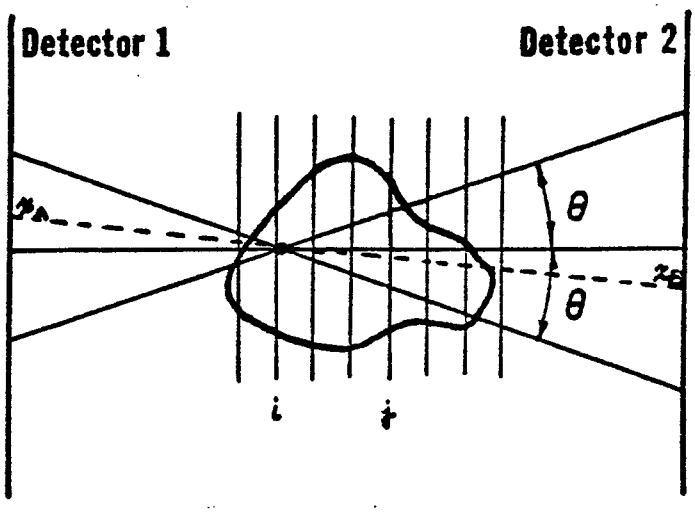


Fig. 1 Large Area Positron Camera. All events within the cone of angle $\Theta$ = 45° are collected.

$$t_j(x) = \sum_{i=1}^{N_t} \int \rho_i(x')\, h_{ij}(x-x')\, dx' \qquad j=1\ldots N_t \qquad (1)$$

We have chosen h to be space-invariant in the x direction which ensures that the Fourier transform of this equation gives a linear equation in the transformed variables for each spatial frequency u.

$$T_j(u) = \sum_{i=1}^{N_t} R_i(u)\, H_{ij}(u) \qquad j=1\ldots N_t \qquad (2)$$

This can be inverted for all spatial frequencies except u = 0

$$R_k(u) = \sum_{j=1}^{N_t} T_j(u)\, H^{-1}_{jk}(u) \qquad k=1\ldots N_t \qquad (3)$$

The u = 0 component is undetermined which means that the inverse Fourier transform of R, the solution to the source distribution, is not known to within an additive constant. This constant can be determined by a priori knowledge that the source distribution is zero outside a given range in x.

Solutions to Eq. 1 are unstable with respect to small errors in the tomograms.[3] When perfect tomograms are used one indeed gets accurate reconstructions. When errors are present due, for instance, to statistical fluctuations, the above exact solution is subject to oscillations. These oscillations can be considerably reduced in a technique due to Phillips and Twomey.[4]

If Eq. 1 is solved using tomograms which differ from the experimental values to within some error value, presumably a value within known experimental error, one can choose from the family of solutions which results, that solution which is the smoothest for a given total error. The resulting smoothest solution is formally the same as Eq. 3 if $H^{-1}$ is replaced by the matrix $(H^tH + \gamma C)^{-1}H^t$. The parameter $\gamma$ is a Lagrangian multiplier which is proportional to the total error

allowed in the tomograms. The matrix C incorporates the smoothness condition. In the cases calculated in our paper C provides for a minimum in a second difference expression, in the z direction, for the reconstructions.

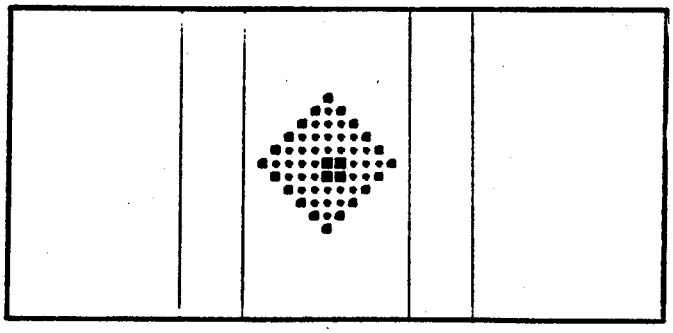

Fig. 2 Phantom used to generate positron events. The detectors are at top and bottom.

## Calculations and Results

The phantom of Fig. 2, with relative intensities of 1, 2, and 4, was used to generate positron events randomly distributed within a cone of 45° angle. Back-projected tomograms were formed from these events on those 11 horizontal lines, 64 pixels wide, which passed through the phantom parallel to the detectors. Eight sets of tomograms were generated, one for each value of n, the number of events/pixel for unit phantom intensity, ranging from 50 through 6400 in powers of two. Since the average intensity of the phantom is 1.52 the average number of events/pixel is 1.52 n. Pixels of equal intensity were made to generate equal numbers of events. Only in the final calculation of signal/noise was the normal statistical variation in positron intensity in a given pixel included. This variation is easily calculated and is statistically independent of the direction of the annihilation gamma rays. For convenience, the annihilation gammas from a source point were generated with a flat distribution on the detector faces instead of with a geometrical distribution. There should be little difference in the effect of the two distributions since they are roughly similar in shape and, with the use of an angular dependent weighting factor for the geometrical distribution events, both will give a flat point response function.

A number of sets of inverses were made, with no smoothing ($\gamma = 0$), and with widely varying values of the smoothing parameter $\gamma$. The additive constant for each line of a reconstruction was determined, in all cases, by a least squares fit of the image + constant to zero in the 5-pixel bands on either side of the phantom (Fig. 2). Finally, to enable us to calculate $\sigma$, the standard deviation/pixel of the reconstruction relative to the phantom, the image was multiplied by a constant and fitted by least squares to the phantom over the area of the phantom.

Using this procedure, 11-line 'exact' tomograms ($n = \infty$) were reconstructed. With no smoothing the image was indistinguishable from the phantom (Fig. 2) and $\sigma$ was 0.000. Fig. 3 is a reconstruction with smoothing ($\gamma = .003$ and $\sigma = .386$). (Values for $\sigma$ should be compared with the average value of the reconstruction over the phantom of 1.52.) For $n = \infty$ all smoothing gives images which are worse than with no smoothing.

For finite numbers of events/pixel this situation is reversed (Fig. 4). The image fidelity of all reconstructions gets better as the smoothing parameter increases from zero until it reaches a point of optimum

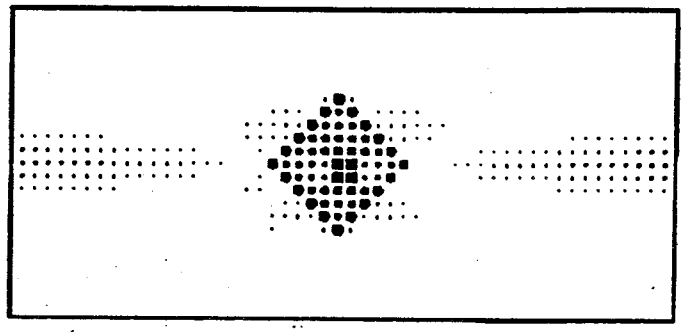

Fig. 3 Reconstruction of the phantom using $N_t = 11$ tomograms, $n = \infty$ events/pixel, and $\gamma = .003$.

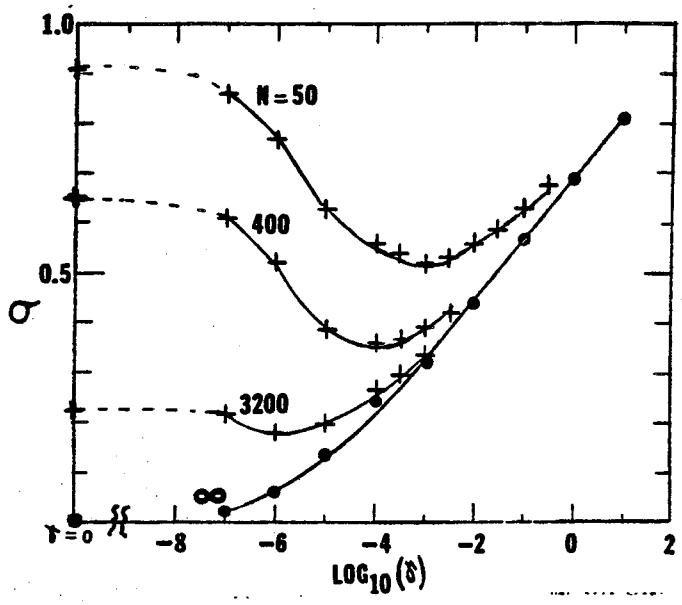


Fig. 4 The standard deviation/pixel, $\sigma$, as a function of the smoothing parameter $\gamma$, for various numbers, n, of events/pixel.

smoothing, $\sigma_{min}$. As $\gamma$ increases beyond this point the distortions allowed by $\gamma$ dominate over any increase of smoothness.

The use of the Phillips-Twomey technique for reducing the oscillations inherent in the solution of Eq. 1 depend on being able to make the optimum choice for $\gamma$. This optimum $\gamma$, the one producing the reconstruction with the best fidelity for the phantom we have used, is plotted in Fig. 5 as a function of the number of events/pixel used to generate the tomograms.

We have not yet investigated the stability of the curve of Fig. 5 against changes in phantom shape and size. Theory shows that $\gamma$ depends directly on the total error allowed in the search for the smoothest solution and is not strongly dependent on the particular tomograms involved.

The improvement in the reconstruction which can be made by using optimum smoothing is shown in Fig. 6 as a function of the number of events/pixel and also in Table I. This increase in fidelity of the reconstructions is greatest in the lower statistics images, about a factor of 1.8 for n = 50-400 events/pixel in the region normally used in the nucear medicine imaging.

Gamma-ray time-of-flight information can be used to give further improvements in the reconstructions. There seems little hope in the foreseeable future that timing techniques will enable localization of the annihilation positron to the one or two centimeter spatial

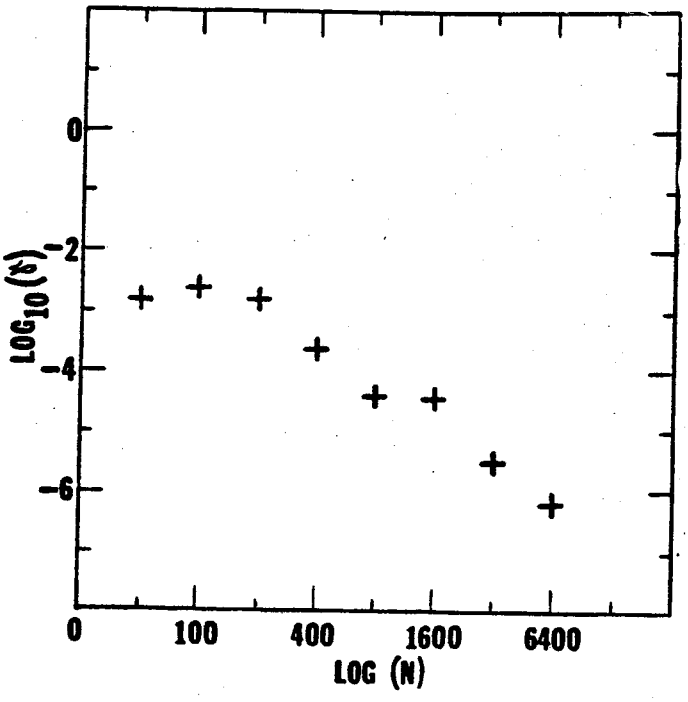


Fig. 5 The parameter $\gamma$ for optimum smoothing as a function of the number of events/pixel.

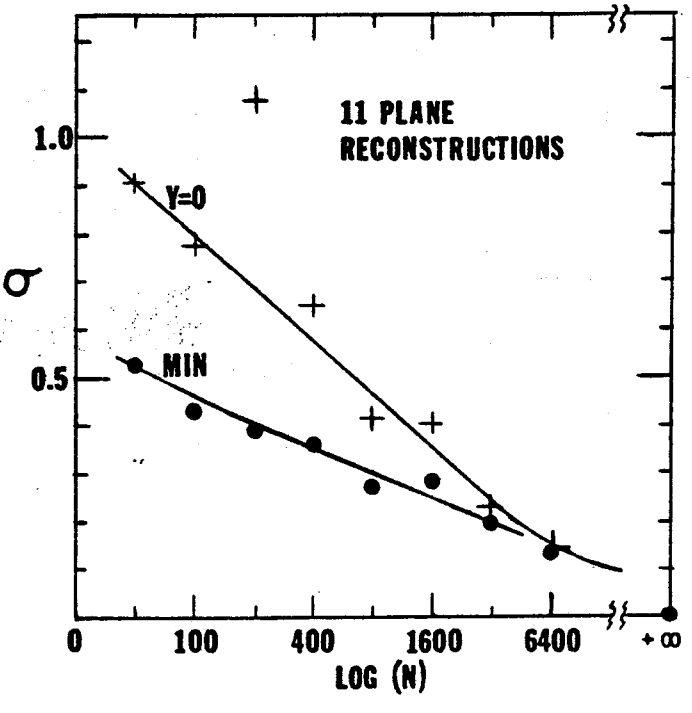


Fig. 6 The standard deviation of reconstructions with $N_t$= 11 tomograms, using no smoothing ($\gamma$=0) and with optimum smoothing ($\sigma_{min}$) for various events/pixel.

resolutions obtained and thus eliminate any necessity for reconstructions. One can only hope that timing information can be used to reduce the source volume contributing to a reconstruction with a corresponding decrease in noise.

Since timing information can be used to select, out of all events collected, just those events within the source coming from a given slab with a certain thickness we have made reconstructions of our phantom using less than its full 11-line extent. The number of lines selected, $N_{tof}$ would depend on the ratio of the depth resolution for time-of-flight to the spatial depth resolution of the camera. Back-projection

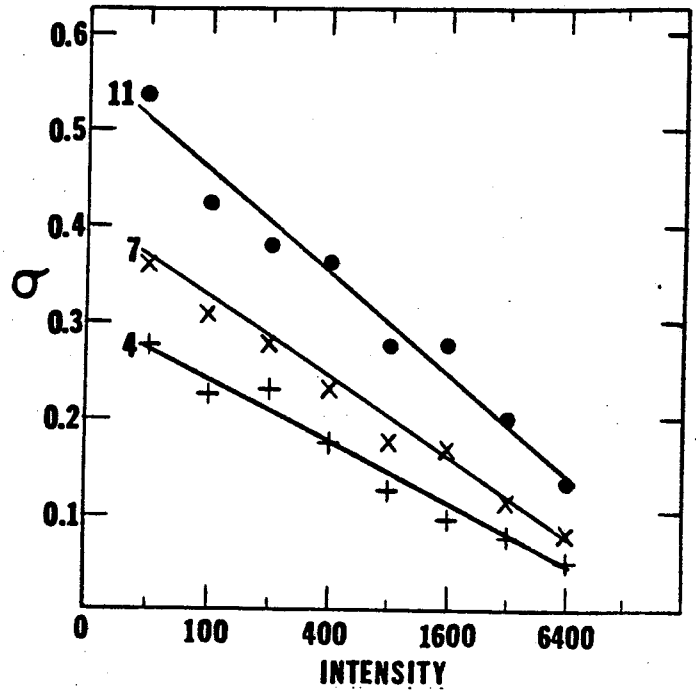


Fig. 7 Improvement in reconstructions using Time-of-Flight. The optimum standard deviation as a function of events/pixel using $N_t$ = 11 and $N_{tof}$ = 7 and 4.

tomograms were made from sources in the phantom which occurred within a window of $N_{tof}$ contiguous lines. Reconstructions were built up by averaging the reconstructions obtained as this window moved over the phantom. Results of these reconstructions are shown in Fig. 7 and also in Table I. When $N_{tof}$ = 4 and thus only 4 parts out of 11 of the phantom was contributing to any sub-reconstruction the reduction in $\sigma_{min}$ was about a factor of 1.9.

Also shown in Table I are figures for the signal/noise ratio, averaged over the area of the phantom, for the optimally smoothed reconstructions as a function of the number of events/pixel. These figures are the full signal/noise ratio for these reconstructions since they incorporate the statistical variation in intensity of pixels in the phantom. When compared with this statistical variation (the last line of Table I) the reconstructions show a magnification of purely statistical noise by a factor of from 3 ( n=50 events/pixel) to 6 ( n=400 events/pixel).

Reconstruction using n = 100 events/pixel (corresponding to an average over the phantom of 150 events/pixel) are shown in Fig. 8. Results for 11 tomogram reconstructions are shown for no smoothing and for optimum smoothing and for a time-of-flight reconstruction with a window of 4 tomograms. Profiles through the central section of the last two reconstructions are shown in Fig. 9.

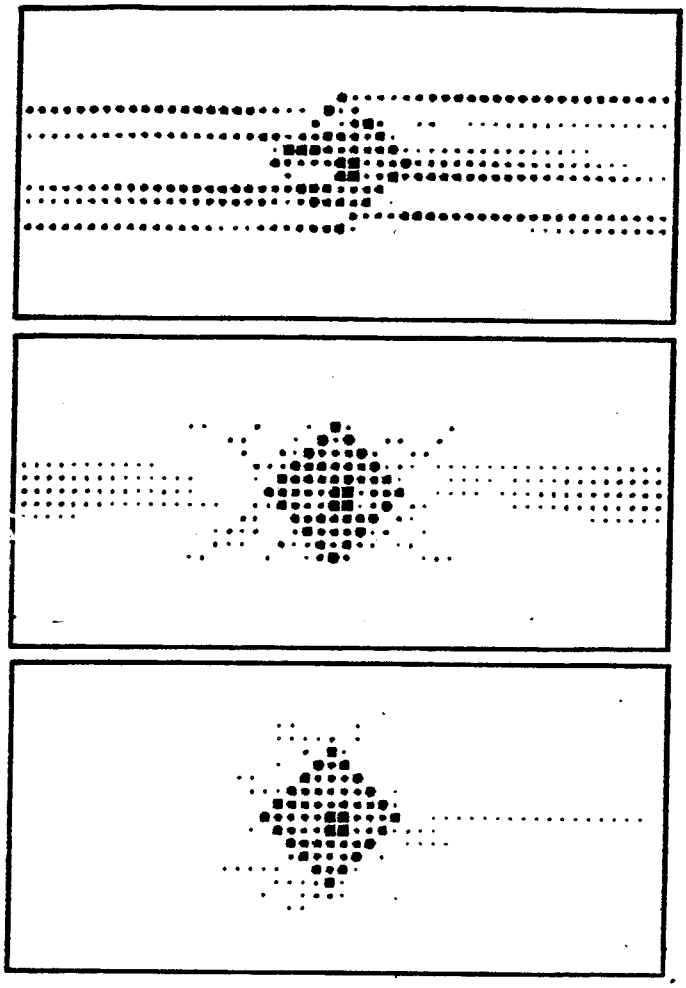

Fig. 8 Reconstructions with n = 100 events/pixel. A) $N_t$ = 11, with no smoothing. B) $N_t$ = 11 with optimum smoothing ($\gamma$ = .003). C) Time-of-Flight $N_{tof}$ = 4 with optimum smoothing ($\gamma$ = .001).

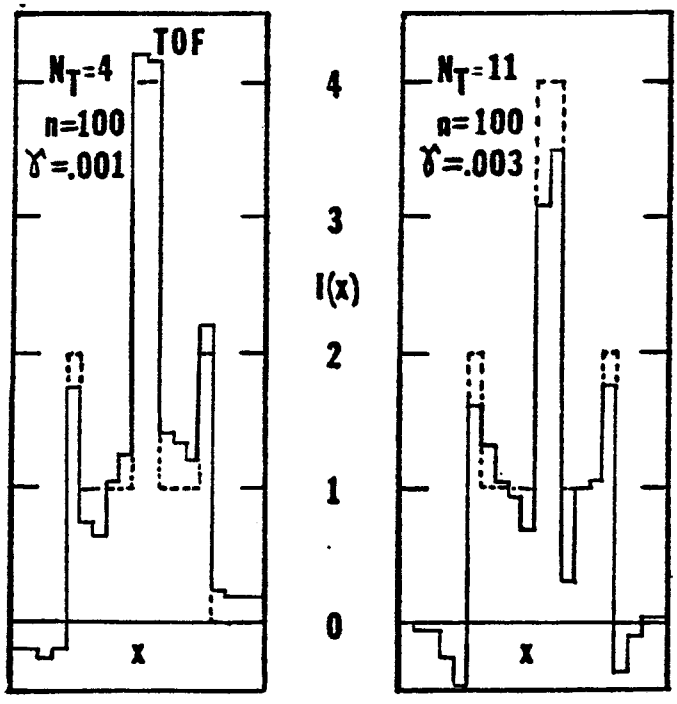


Fig. 9 Profiles, through the central section, of reconstructions with and without time-of-flight, for 100 events/pixel.

Table I. $\sigma$, image standard deviations from the input phantom, with no smoothing ($\gamma$=0) and with optimum smoothing ($\sigma_{min}$), for various numbers of tomograms used and numbers of events in the tomograms. S/N, the signal/noise ratio for the optimally smoothed images and that expected for the phantom with statistical intensity variations only.

| | | n (events/pixel) 50 | 100 | 200 | 400 | 800 |
|---|---|---|---|---|---|---|
| $N_t$ = 11 | $\sigma(\gamma=0)$ | .845 | .716 | .819 | .687 | .358 |
| | $\sigma_{min}$ | .545 | .426 | .419 | .355 | .227 |
| $N_{tof}$=7 | $\sigma(\gamma=0)$ | .621 | .420 | .582 | .465 | .214 |
| | $\sigma_{min}$ | .355 | .318 | .296 | .211 | .149 |
| $N_{tof}$=4 | $\sigma(\gamma=0)$ | .451 | .291 | .409 | .329 | .148 |
| | $\sigma_{min}$ | .267 | .229 | .321 | .141 | .107 |
| $N_t$ = 11 | S/N | 2.7 | 3.4 | 3.6 | 4.2 | 6.6 |
| $N_{tof}$ = 7 | S/N | 3.9 | 4.5 | 4.9 | 6.9 | 9.8 |
| $N_{tof}$ = 4 | S/N | 4.8 | 5.9 | 6.2 | 9.9 | 13.2 |
| Statistical | S/N | 8.7 | 12.3 | 17.5 | 24.7 | 35.0 |

## References


1. M.M. Ter Poggossian et al, Time-of-Flight Assisted Positron Emission Tomography, J.C.A.T. 5 227-239 (1981)

2. L.T. Chang, B. Macdonald, and V. Perez-Mendez, Axial Tomography and Three Dimensional Image Reconstruction, IEEE Trans. Nucl. Sci. NS-23 568-572 (1976)

3. K.C. Tam et al, Limited Angle 3-D Reconstructions from Continuous and Pinhole Projections, IEEE Trans. Nucl. Sci. NS-27 445-458 (1980).

4. B.L. Phillips, A Technique for the Numerical Solution of Certain Integral Equations of the First Kind, J. A.C.M. 9 84-97 (1962). S. Twomey, On the Numerical Solution of Fredholm Integral Equations of the First Kind of the Inversion of the Linear System Produced by Quadrature



This work was supported by the U.S. Department of Energy under Contract No. W-7405-ENG-48.